SPECTRAL METHODS FOR FORWARD-PROPAGATING WATER WAVES IN CONFORMALLY-MAPPED CHANNELS

Robert A. Dalrymple, James T. Kirby and P. A. Martin

RESEARCH REPORT NO. CACR-94-01

January 1994

CENTER FOR APPLIED COASTAL RESEARCH

Ocean Engineering Laboratory
University of Delaware
Newark, Delaware 19716

Spectral methods for forward-propagating water waves in conformally-mapped channels

Robert A. Dalrymple[†] James T. Kirby[†] P. A. Martin[‡]

Abstract

The prediction of wave fields in domains with complicated geometries may be aided by the use of conformal mapping, which simplifies the shape of the domain. In this conformal domain, parabolic models have been used previously to treat wave problems. In Cartesian coordinates, the angular spectrum model, based on a Fourier transform in the direction perpendicular to the principal propagation direction, has been shown to handle, in principle, a wider range of wave directions than the parabolic model.

Here, the extension of the angular spectrum model to conformally-mapped domains with impermeable lateral boundaries is shown. Next, the Fourier-Galerkin method is developed; this is identical to the angular spectrum model in Cartesian coordinates, but differs in the conformal domain. Finally, a Chebyshev-tau model is developed, based on using Chebyshev polynomials rather than trigonometric functions as a basis. For all models, forward-propagation equations are derived, by splitting the governing elliptic equations into first-order equations. Examples of all methods are shown for a simple conformal mapping that permits the study of waves in a diverging channel and in a circular channel. The forward-propagation models are shown to be optimal for methods that use eigenfunctions for the lateral transform and less accurate for others.

1 Introduction

Wave modelling in regions where the boundaries are uncomplicated can be easily carried out by a variety of means. For over a decade, parabolic modelling, based on finite-difference methods, has been used with success to examine refraction, diffraction and shoaling of short waves over large coastal areas [24], [17], [18]. More recently, angular spectrum modelling has been used [26], [7], [8], [11]. As originally conceived [2], the angular spectrum model involves the decomposition of an incident wave field into plane waves, which then are allowed to propagate into the domain. The resulting wave field is the superposition of these plane waves. This technique is carried out by Fourier transforming the governing equation and initial condition in the lateral direction, and then solving the resulting one-dimensional

[†]Center for Applied Coastal Research, Department of Civil Engineering, University of Delaware, Newark, DE 19716.

[‡]Department of Mathematics, University of Manchester, Manchester M13 9PL, England.

equations for the Fourier modes, which are then superimposed for the final wave field. This method of expressing the wave field as a Fourier integral or a trigonometric series has the potential advantage of permitting wider angles of wave approach when compared to parabolic modelling, which is constrained by a preferred propagation direction. Also, the angular spectrum methodology (see [9] for a review) can be applied to weakly nonlinear water waves [28], shallow water Boussinesq waves [16], and directional spectra [14], [27].

For problems that are periodic in one direction, the Fourier trigonometric basis is optimal for the series expansion of the solution in that direction. For other problems, Chebyshev polynomials are usually preferred. For example, Boyd [3] has treated a number of nonlinear wave problems with these polynomials, whilst Panchang and Kopriva [23] have used them in both horizontal directions in a collocation method for solving the elliptic mild-slope equation. However, the Chebyshev polynomials do not satisfy our lateral boundary conditions, so an equivalent method to the Fourier-Galerkin method will not be possible; a Chebyshev-tau method overcomes this difficulty by using two additional equations to enforce the boundary conditions and is very similar in application [20].

Wave prediction in realistic coastal situations is often complicated by the layout of breakwaters and other hard structures coupled with variable depths and currents. These complicated situations can often be simplified if a coordinate transformation is used that conforms to the physical boundaries. Hence, we consider a general class of conformal transformations from the Cartesian coordinates (x, y) into boundary-fitted coordinates (u, v), so that no-flow boundary conditions can be applied on coordinate lines. We then investigate models for forward wave propagation, developed in the transformed domain.

Boundary-fitted coordinates have been used extensively in other fields with good success [29], [30]. In the field of wave propagation, Liu and Boissevain [21] transformed the parabolic model into a non-orthogonal coordinate system to examine the propagation of waves in a diverging channel (harbor entrance). Kirby [15] showed that it is important to determine the parabolic model within the mapped domain. Tsay *et al.* [31] developed low-order parabolic approximations for several geometries, while Kirby *et al.* [19] developed parabolic models for a general conformal case for both small- and large-angle parabolic approximations. They also show results for two specific geometries and presented laboratory results for the case of the diverging breakwater.

Here we develop the forward-propagation equations for Fourier-Galerkin, angular spectrum and Chebyshev-tau models in conformal domains, and compare the results to exact solutions for two simple planforms – waves between diverging breakwaters and waves in a circular channel; these are the same geometries as used in [19].

2 Theory: Cartesian coordinates

The governing equation for the propagation of linear waves in constant water depth is the two-dimensional Helmholtz equation,

$$\frac{\partial^2 \phi}{\partial x^2} + \frac{\partial^2 \phi}{\partial y^2} + k^2 \phi = \nabla^2 \phi + k^2 \phi = 0, \tag{1}$$

where (x, y) are the horizontal Cartesian coordinates and the total wave potential is

$$\mathrm{Re}\left\{\phi(x,y)\frac{\cosh k(h+z)}{\cosh kh}\,\mathrm{e}^{-\mathrm{i}\omega t}\right\}.$$

The mean free surface is at $z = 0$ and the bottom is at $z = -h$. The wavenumber k is related to the water depth h and the angular frequency of the wave ω by the dispersion relationship,

$$\omega^2 = gk\tanh kh.$$

We are interested in situations in which waves are primarily propagating in the $+x$ direction within a domain of given width. As an example, for a straight channel of width $2b$, with impermeable walls at $y = \pm b$, we can use separation of variables to solve for the velocity potential. Assuming $\phi(x, y) = X(x)Y(y)$, yields two equations

$$X'' + (k^2 - \lambda^2)X = 0, \tag{2}$$

$$Y'' + \lambda^2 Y = 0. \tag{3}$$

For no-flow lateral boundary conditions, we have $Y'(y) = 0$ at $y = \pm b$; therefore we have a Sturm-Liouville problem in the y-direction. The eigenvalues are $\lambda_n = \frac{1}{2}n\pi/b$ and the eigenfunctions are $\{\cos[\lambda_n(y + b)]\}$, $n = 0, 1, 2, \ldots$. The corresponding solutions of (2) are easily shown to be exponential functions. Finally, summing all the possible solutions together, we obtain

$$\phi(x,y) = \sum_{n=-\infty}^{\infty} a_n \exp\left\{\pm\mathrm{i}x\sqrt{k^2-\lambda_n^2}\right\}\cos[\lambda_n(y+b)], \tag{4}$$

where the a_n are constants. The forward-propagating waves will be associated with the positive sign in the exponent. Also, note that for values of $\lambda_n > k$, the forward-propagating wave modes decay exponentially with $+x$.

Another method of solving the two-dimensional equation (1) is to use a transform in the lateral direction (y), thus reducing it to one-dimensional equations. A general transform pair can be described by

$$\Psi_n(x) = \mathcal{T}_\psi[\phi(x,y)] = \int_{-b}^{b}\phi(x,y)\psi_n(y)w(y)\,dy, \quad n = 0, 1, 2, \ldots, \tag{5}$$

$$\phi(x,y) = \mathcal{T}_\psi^{-1}[\Psi(x)] = \sum_{n=0}^{\infty}\Psi_n(x)\psi_n(y) \qquad \text{for } -b < y < b, \tag{6}$$

where $\{\psi_n(y)\}$, $n = 0, 1, 2, \ldots$, is a set of functions that are orthogonal (with weight w) over the range $-b \le y \le b$, and $\Psi_n(x)$ are the amplitudes of these orthogonal functions. Two common choices for $\psi_n(y)$ are trigonometric functions (Fourier transforms) and Chebyshev polynomials.

To proceed, we transform (1) into a set of equations for the amplitudes:

$$\frac{d^2\Psi_n(x)}{dx^2} + \mathcal{T}_\psi\left[\frac{\partial^2\mathcal{T}_\psi^{-1}[\Psi]}{\partial y^2}\right] + k^2\Psi_n(x) = 0, \quad n = 0, 1, 2, \ldots. \tag{7}$$

Once these equations have been solved for Ψ_n, the inverse transform (6) is used to find the solution, $\phi(x, y)$.

2.1 Angular spectrum and Fourier-Galerkin modelling

Here, we will use the Fourier transform for a domain of width $2b$, so that $\psi_n = \cos[\lambda_n(y+b)]$, with $\Psi_n = f_n$, $w = 1$, and $\lambda_n = \frac{1}{2}n\pi/b$. This gives

$$f_n(x) = \mathcal{T}_F[\phi(x,y)] = \frac{1}{2b}\int_{-b}^{b} \phi(x,y)\cos[\lambda_n(y+b)]\,dy, \quad n = 0,1,2,\ldots, \tag{8}$$

$$\phi(x,y) = \mathcal{T}_F^{-1}[f] = \sum_{n=0}^{\infty} \epsilon_n f_n(x)\cos[\lambda_n(y+b)], \qquad \text{for } -b < y < b, \tag{9}$$

where $\epsilon_0 = 1$ and $\epsilon_n = 2$ for $n \geq 1$. The $f_n(x)$ are the Fourier modal amplitudes. Since

$$\mathcal{T}_F\left[\frac{\partial^2\phi}{\partial y^2}\right] = -\lambda_n^2 f_n,$$

the governing equations for the Fourier modes simplify. Thus, transforming the Helmholtz equation (1), we obtain

$$\frac{d^2 f_n(x)}{dx^2} + (k^2 - \lambda_n^2)f_n(x) = 0, \quad n = 0,1,2\ldots. \tag{10}$$

This equation shows that each Fourier mode evolves independently of all the others. Solving (10) gives

$$f_n(x) = a_n \exp\left\{\pm \mathrm{i}x\sqrt{k^2 - \lambda_n^2}\right\}, \qquad \text{for } n = 0,1,2,\ldots;$$

we take the $+$ as we are interested in propagation in the $+x$ direction. Only those modes for which $\lambda_n < k$ represent progressive wave trains; the remainder decay with x. Therefore, the solution procedure is simplified (in the far field) by determining only the progressive modes.

The inverse Fourier transform, (9), provides the final solution,

$$\phi(x,y) = \sum_{n=0}^{\infty} \epsilon_n a_n \exp\left\{\mathrm{i}x\sqrt{k^2 - \lambda_n^2}\right\}\cos[\lambda_n(y+b)].$$

The constants a_n are found from the Fourier transform of the 'initial condition', $\phi(0,y)$: $a_n = \mathcal{T}_F[\phi(0,y)]$. This solution comprises the angular spectrum, which is the superposition of many plane wave trains, each travelling in a direction given by $\tan^{-1}(\lambda_n/\sqrt{k^2 - \lambda_n^2})$. It can also be viewed as the superposition of the fundamental modes of the Laplace equation. This is the *angular spectrum model* for a channel.

The angular spectrum model is indistinguishable in Cartesian coordinates from the separation of variables solution, or an eigenfunction expansion method, since the Fourier series are in fact the eigenfunctions in the lateral direction. Dalrymple [6] used these series expansions for ϕ to examine waves past channel transitions, and Dalrymple and Martin [10] examined waves through a line of offshore breakwaters.

The Fourier-Galerkin model assumes that the potential can be expanded in a trigonometric series (here, cosines) in the lateral direction. Orthogonality of the trigonometric functions

is used to develop the equations governing the modal amplitudes. A Fourier transform in the lateral direction gives an identical result, therefore we will use the Fourier transform to derive the equations below. In Cartesian coordinates the Fourier–Galerkin method is also the same as the angular spectrum model.

2.2 Chebyshev-tau method

This method begins with

$$\psi_n(y) = T_n(Y) \quad \text{where } Y = y/b, \tag{11}$$

and T_n is a Chebyshev polynomial. The Chebyshev transform and its inverse are

$$c_n(x) = \mathcal{T}_C[\phi(x,y)] = \frac{\epsilon_n}{\pi}\int_{-1}^{1} \frac{\phi(x,bY)\,T_n(Y)}{\sqrt{1-Y^2}}\,dY, \quad n = 0,1,2,\ldots, \tag{12}$$

$$\phi(x,y) = \mathcal{T}_C^{-1}[c(x)] = \sum_{n=0}^{\infty} c_n(x)\,T_n(Y), \qquad \text{for } -1 < Y < 1. \tag{13}$$

For the Chebyshev polynomials, the second derivative does not behave as conveniently as in the Fourier transform. However it can be rewritten in a form which is computationally more convenient (and accurate) for large values of n [5, p. 69]:

$$\frac{\partial^2\phi}{\partial y^2} = \sum_{n=0}^{\infty} c_n(x)\frac{d^2T_n(Y)}{dy^2} = \frac{1}{b^2}\sum_{n=0}^{\infty} c_n^{(2)}\,T_n(Y) \tag{14}$$

where

$$c_n^{(2)} = 2\epsilon_n \sum_{l=1}^{\infty} l(n+l)(n+2l)\,c_{n+2l}(x). \tag{15}$$

The transformed equation is now

$$\frac{d^2c_n}{dx^2} + k^2c_n(x) + \frac{1}{b^2}c_n^{(2)} = 0, \quad n = 0,1,2,\ldots, \tag{16}$$

which is a coupled (through the second derivative) system of equations for the modal amplitudes.

Note that $\psi_n(y)$, defined by (11), does not satisfy the no-flow conditions on the walls; in fact,

$$\psi_n'(-b) = T_n'(-1) = n^2(-1)^{n+1} \quad \text{and} \quad \psi_n'(b) = T_n'(+1) = n^2.$$

In order to enforce the boundary conditions, we use the Chebyshev-tau method [5], which is discussed in § 4.3.

The Chebyshev-tau method does not offer any advantages for the Helmholtz equation in Cartesian coordinates since *all* modes are progressive implying that, numerically, many terms must be retained in (13). However, the situation may be different for other coordinate systems or for other equations. Before investigating these possibilities, we introduce the forward-propagation models.

2.3 Forward-propagation models

The governing equation (7) is a second-order ordinary differential equation that requires two boundary conditions. The initial conditions for the amplitudes are readily found by transforming the initial condition, while the other boundary condition, for large x, say, is often unknown *a priori*. Dalrymple and Kirby [8], using Fourier transforms, surmounted this problem by splitting the Fourier amplitude $f_n(x)$ into forward-propagating and backward-propagating terms: $f_n = f_n^+ + f_n^-$; these are associated with the positive and the negative signs in the exponent of (4). This leads to first-order differential equations in the split variables, which are also faster to solve numerically than the original second-order equation.

Assume that

$$\begin{aligned}\frac{df_n^+}{dx} &= \mathrm{i}\sqrt{k^2-\lambda^2}\, f_n^+ + F_n(x),\\ \frac{df_n^-}{dx} &= -\mathrm{i}\sqrt{k^2-\lambda^2}\, f_n^+ - F_n(x),\end{aligned}$$

where the function F_n is unknown *a priori*. Substituting into (10) gives $F_n(x) = 0$, so that the second-order equation is split exactly and the forward-propagating mode is correctly given by

$$\frac{df_n^+}{dx} = \mathrm{i}\sqrt{k^2-\lambda^2}\, f_n^+.$$

The solution to this first-order equation depends on the initial condition only (meaning we can neglect the unknown downwave boundary condition). Moreover, it is exactly the same as that given by separation of variables applied to the Helmholtz equation, showing again that the splitting procedure is exact for this equation.

For the Chebyshev-tau method, the splitting in the transform domain follows the same procedure as before, except that the assumed splitting is different because of the nature of the second derivative in y:

$$\begin{aligned}\frac{dc_n^+}{dx} &= \mathrm{i}k\, c_n^+ + F_n(x),\\ \frac{dc_n^-}{dx} &= -\mathrm{i}k\, c_n^- - F_n(x).\end{aligned}$$

Substituting into (16), the forward-propagating equation is found to be

$$\frac{dc_n^+(x)}{dx} = \mathrm{i}k\, c_n^+(x) + \frac{\mathrm{i}}{2kb^2}\, c_n^{(2)} = 0,$$

where only the c_n^+ are used to calculate $c_n^{(2)}$. If we used the first form of the second derivative in (14), this equation would be

$$\frac{dc_n^+(x)}{dx} = \mathrm{i}k\, c_n^+(x) + \frac{\mathrm{i}}{2k}\mathcal{T}_C\left[\frac{\partial^2 \mathcal{T}_C^{-1}[c]}{\partial y^2}\right] = 0.$$

The inverse transform of this equation is

$$\frac{\partial \phi}{\partial x} = \mathrm{i}k\phi + \frac{\mathrm{i}}{2k}\frac{\partial^2 \phi}{\partial y^2} = 0$$

which is the small-angle parabolic representation of the Helmholtz equation. Small-angle parabolic models are known to be inaccurate for waves that propagate at large angles to the x-axis. This appears to be a serious consequence of splitting the Chebyshev equation, potentially limiting its effectiveness in forward-propagating models. This same result applies to the variable-depth (mild-slope) equation.

3 Theory: conformal mapping

In the physical domain, the velocity potential, $\phi(x, y)$ is found by solving the Helmholtz equation in the given complicated geometry. Alternatively, we can map the problem into a conformal domain, which is identified with the independent variables, $u(x, y)$ and $v(x, y)$. The dependent variable becomes $\phi(u, v)$. The mapping procedure is described in the Appendix (following [19] or, more generally, [12]). For all cases, the channel sidewalls will be mapped into $v = \pm v_b$.

The resulting governing equation in the conformal domain is much the same as that in Cartesian coordinates,

$$\frac{\partial^2 \phi}{\partial u^2} + \frac{\partial^2 \phi}{\partial v^2} + k^2 J \phi = 0, \tag{17}$$

with the exception of the presence of J, which is the Jacobian of the transformation, defined by

$$J(u, v) = \frac{\partial x}{\partial u}\frac{\partial y}{\partial v} - \frac{\partial x}{\partial v}\frac{\partial y}{\partial u}. \tag{18}$$

We can only obtain separated solutions of (17) if $k^2 J$ is of the form

$$k^2 J(u, v) = \mathcal{J}_1(u) + \mathcal{J}_2(v).$$

Then, with $\phi(u, v) = U(u)V(v)$, we obtain the following equations for U and V:

$$U'' + (\mathcal{J}_1 - \lambda^2)U = 0, \tag{19}$$

$$V'' + (\mathcal{J}_2 + \lambda^2)V = 0. \tag{20}$$

In particular, if $\mathcal{J}_2 \equiv 0$, the lateral eigenmodes for the channel are

$$V_n(v) = \cos\left[\lambda_n(v + v_b)\right] \qquad \text{with} \qquad \lambda_n = \tfrac{1}{2}n\pi/v_b, \tag{21}$$

just as for the Cartesian case. Alternatively, if $\mathcal{J}_1 \equiv 0$, then we obtain $U(u) = \mathrm{e}^{\mathrm{i}\lambda u}$ as a propagating mode; here, we have replaced λ^2 by $-\lambda^2$, giving

$$V'' + (\mathcal{J}_2 - \lambda^2)V = 0$$

as the equation for the lateral modes.

3.1 Examples

A logarithmic conformal mapping will be used here to illustrate the various spectral approaches to wave modelling. This mapping converts radial lines and circles about the origin in the physical domain into orthogonal straight lines in the mapped domain.

3.1.1 The diverging channel

The first example is a constant depth, radially diverging channel with straight vertical impermeable sidewalls. The mapping is $w = \ln(z/r_0)$, where $w = u + \mathrm{i}v$, $z = x + \mathrm{i}y$ and r_0 is the distance from the origin to the mouth of the channel. The mapping can be rewritten as $u = \ln(r/r_0)$ and $v = \theta$, which, with the exception of the presence of the logarithm, looks like a polar-coordinate transformation. The channel sidewalls lie on $v = \pm v_b = \pm\theta_\ell$. In terms of x and y, the inverse mapping gives $z = r_0 \mathrm{e}^w$, or, $x = r_0\,\mathrm{e}^u \cos v$ and $y = r_0\,\mathrm{e}^u \sin v$. In the z-plane, the waves are supposed to propagate in the positive x-direction, while in the mapped domain, the waves will travel primarily in the positive u-direction. See Figure 1a.

The Jacobian of the transformation is $J = r_0^2\,\mathrm{e}^{2u}$, which is a function of u only. Thus, $\mathcal{J}_2 \equiv 0$, whence $V(v) = \cos[\lambda(v + v_b)]$ and

$$U'' + [(kr_0\,\mathrm{e}^u)^2 - \lambda^2]U = 0,$$

which has the general solution

$$U(u) = AJ_\lambda(kr_0\,\mathrm{e}^u) + BY_\lambda(kr_0\,\mathrm{e}^u),$$

where J_λ and Y_λ are Bessel functions. For rigid walls at $v = \theta = \pm\theta_\ell$ (so that $v_b = \theta_\ell$), and for waves propagating in the direction of u increasing, we readily obtain the solution

$$\phi(r,\theta) = \sum_{n=0}^{\infty} a_n H^{(1)}_{\beta_n}(kr)\cos\beta_n(\theta + \theta_\ell), \tag{22}$$

where $H^{(1)}_\lambda = J_\lambda + \mathrm{i}Y_\lambda$ and $\lambda = \beta_n$, with $\beta_n = \frac{1}{2}n\pi/\theta_\ell$.

Given the potential at $r = r_0$ as $G(\theta)$, the modal amplitudes are

$$a_m = \frac{\epsilon_m}{2\theta_\ell\, H^{(1)}_{\beta_n}(kr_0)} \int_{-\theta_\ell}^{\theta_\ell} G(\theta)\cos\beta_m(\theta + \theta_\ell)\,d\theta \qquad \text{for } m = 0, 1, 2, \ldots. \tag{23}$$

For the case of a planar wave train entering into a diverging channel centered about $\theta = 0$, we take $G(\theta) = \exp(\mathrm{i}kr_0\cos\theta)$, corresponding to normal incidence.

We note that (22) is the exact linear solution; it can also be obtained by separation of variables of (1) in plane polar coordinates [19].

3.1.2 The circular channel

The second example is a constant depth channel with vertical sidewalls laid out in a circular planform. Let r_1 and r_2 be the inner and outer radius of the channel, respectively. The waves

are supposed to propagate primarily counter-clockwise in the axial (θ) direction, from the mouth of the channel located at $\theta = -\pi/2$. In the mapped domain, the channel is straight, with the waves again propagating in the positive u-direction, as shown in Figure 1b. Here the conformal map is somewhat different (to keep the same u principal propagation directions): $w = \pi/2 - \mathrm{i}\ln(z/r_\mathrm{m})$, where $r_\mathrm{m} = \sqrt{r_1 r_2}$. This corresponds to $u = \pi/2 + \theta$ and $v = \ln(r_\mathrm{m}/r)$. The outer sidewall of the channel is mapped to $v = -v_b = \ln(r_\mathrm{m}/r_2) = -\frac{1}{2}\ln(r_2/r_1)$, while the inner wall is mapped to $v = v_b$. In terms of z, we have $z = r_\mathrm{m}\mathrm{e}^{\mathrm{i}(w-\pi/2)}$, which leads to $x = r_\mathrm{m}\mathrm{e}^{-v}\sin u$ and $y = -r_\mathrm{m}\mathrm{e}^{-v}\cos u$.

The Jacobian of this transformation is $J = r_\mathrm{m}^2\mathrm{e}^{-2v}$, which is a function of v only. Thus, $\mathcal{J}_1 \equiv 0$, whence

$$U(u) = \mathrm{e}^{\mathrm{i}\lambda u} \tag{24}$$

for propagation in the direction of u increasing. $V(v)$ satisfies

$$V'' + [(kr_\mathrm{m}\mathrm{e}^{-v})^2 - \lambda^2]V = 0, \tag{25}$$

which has general solution

$$V(v) = AJ_\lambda(kr_\mathrm{m}\mathrm{e}^{-v}) + BY_\lambda(kr_\mathrm{m}\mathrm{e}^{-v}).$$

At the outer wall $r = r_2$, we have $v = \frac{1}{2}\ln(r_1/r_2) = -v_b$ and $V'(-v_b) = 0$; therefore

$$V(v) = Y'_\lambda(kr_2)J_\lambda(kr_\mathrm{m}\mathrm{e}^{-v}) - J'_\lambda(kr_2)Y_\lambda(kr_\mathrm{m}\mathrm{e}^{-v}).$$

At the inner wall $r = r_1 < r_2$, we have $v = v_b$ and $V'(v_b) = 0$, giving

$$Y'_\lambda(kr_1)J'_\lambda(kr_2) - J'_\lambda(kr_1)Y'_\lambda(kr_2) = 0. \tag{26}$$

This is an equation for λ. It is known that (26) has discrete roots; call them $\lambda = \alpha_n$, with $n = 0, 1, 2, \ldots$. There are only a finite number of real roots ($0 < \alpha_n < kr_2$); these give the propagating modes. Equation (26) also has an infinite number of purely imaginary solutions; those with positive imaginary parts give the evanescent modes. For a discussion of these solutions, see [4] in the context of curved electromagnetic wave guides, or [25] in the context of acoustics.

Ordering the real eigenvalues from the largest to the smallest, we find that the first eigenvalue corresponds to the zeroth mode, which has no zero crossing in the transverse (radial) direction. Therefore the mode looks like a propagating wave train, but confined to the outer wall; it is the annular equivalent of the 'whispering gallery mode' as it is large on the outer radius and decays rapidly and monotonically in the (negative) r-direction. The next eigenvalue corresponds to the first mode, with one zero crossing, and so on.

In Figure 11, the exact linear solution for the wave field is shown for waves incident into a 180° turn. As the waves enter the channel, they begin to reflect from the outer wall and diffract in the vicinity of the inner wall.

The problem of solving (25), together with $V'(\pm v_b) = 0$, is a Sturm-Liouville problem. Let $V_n(v)$ be a solution corresponding to $\lambda = \alpha_n$,

$$V_n(v) = A_n\left\{Y'_{\alpha_n}(kr_2)J_{\alpha_n}(kr_\mathrm{m}\mathrm{e}^{-v}) - J'_{\alpha_n}(kr_2)Y_{\alpha_n}(kr_\mathrm{m}\mathrm{e}^{-v})\right\} \tag{27}$$

(recall that $r = r_{\mathrm{m}}\mathrm{e}^{-v}$). These eigenfunctions are orthogonal,

$$\int_{-v_b}^{v_b} V_m(v)V_n(v)\,dv = 0 \qquad \text{for } \alpha_m \neq \alpha_n,$$

and the constant A_n can be chosen so that

$$\int_{-v_b}^{v_b} V_n^2(v)\,dv = 1.$$

They are also complete, so that we have

$$\phi(u,v) = \sum_{n=0}^{\infty} a_n\,\mathrm{e}^{\mathrm{i}\alpha_n u}\,V_n(v). \tag{28}$$

At the beginning of the channel, $u = 0$ ($\theta = -\pi/2$) and $\phi(0,v) = G(v)$, say, whence

$$a_n = \int_{-v_b}^{v_b} G(v)V_n(v)\,dv. \tag{29}$$

Again, this solution is exact; it can also be obtained by separation of variables of (1) in plane polar coordinates [19].

4 Numerical modelling in the conformal domain

4.1 Fourier-Galerkin approach

As in [11], where a Helmholtz equation with variable coefficients (arising due to bottom variations) was treated, we define a lateral average of the variable coefficient in the conformal Helmholtz equation (17) by

$$\overline{k^2J}(u) = \frac{1}{2v_b}\int_{-v_b}^{v_b} k^2J(u,v)\,dv. \tag{30}$$

Substituting this into the governing equation (17) gives

$$\frac{\partial^2\phi}{\partial u^2} + \frac{\partial^2\phi}{\partial v^2} + \overline{k^2J}\,(1-\nu)\phi = 0, \tag{31}$$

where

$$\nu(u,v) = 1 - k^2J/\overline{k^2J} \tag{32}$$

incorporates the lateral variability of the original coefficient, k^2J.

We suppose, as before, that the boundaries at $v = \pm v_b$ are impermeable (so that $\partial\phi/\partial v = 0$). Then, the appropriate Fourier-transform pair is the following (cf. (8) and (9)):

$$f_n(u) = \mathcal{T}_F[\phi(u,v)] = \frac{1}{2v_b}\int_{-v_b}^{v_b}\phi(u,v)\cos[\lambda_n(v+v_b)]\,dv, \quad n = 0,1,2,\ldots \tag{33}$$

$$\phi(u,v) = \mathcal{T}_F^{-1}[f(u)] = \sum_{n=0}^{\infty}\epsilon_n f_n(u)\cos[\lambda_n(v+v_b)] \quad \text{for } -v_b < v < v_b. \tag{34}$$

Transforming (31) yields

$$\frac{d^2 f_n}{du^2} + \gamma_n^2 f_n - \overline{k^2 J}\, \mathcal{T}_F[\nu\, \mathcal{T}_F^{-1}[f]] = 0, \qquad n = 0, 1, 2, \ldots, \tag{35}$$

where

$$\gamma_n^2(u) = \overline{k^2 J} - \lambda_n^2 \qquad \text{and} \qquad \lambda_n = \tfrac{1}{2} n\pi / v_b.$$

The set of equations (35) is exactly equivalent to (31), provided the series (34) converges. The last term in (35), which adds complexity to the solution, results from the Fourier transform of a product of two functions of v.

To obtain a forward-propagation model, we separate f_n into forward and backward propagating wave modes as before and keep only the forward-propagating modes to yield

$$\frac{df_n^+(u)}{du} = \left(\mathrm{i}\gamma_n - \frac{1}{2\gamma_n}\frac{d\gamma_n}{du}\right) f_n^+ - \frac{\mathrm{i}\,\overline{k^2 J}}{2\gamma_n} \mathcal{T}_F[\nu\, \mathcal{T}_F^{-1}[f^+]], \quad n = 0, 1, 2, \ldots. \tag{36}$$

This final set of equations governs the propagating Fourier modes. The equations are approximate due to the neglect of the backward-propagating modes that occur in the last term; this term couples all the modes and can result in the growth of modes that may have been originally zero at $u = 0$.

The initial conditions on $f_n(u)$ are provided by a Fourier transform of the given initial condition, $\phi(0, v) = G(v)$, say, giving

$$f_n(0) = \frac{1}{2v_b} \int_{-v_b}^{v_b} G(v) \cos\left[\lambda_n(v + v_b)\right] dv \qquad n = 0, 1, 2, \ldots.$$

Suppose that $\nu \equiv 0$, that is, $k^2 J$ is independent of v, the lateral coordinate. Then, as we have seen in § 3 (the case $\mathcal{J}_2 \equiv 0$), (31) is separable: the lateral eigenfunctions of the problem, $V_n(v)$, satisfying the sidewall conditions, $V'(v) = 0$ at $v = \pm v_b$, are given by (21). In other words, for this particular case, the actual lateral eigenfunctions are the same cosines as used in the Fourier-transform pair, (33) and (34). It follows that the convergence of the method is guaranteed. However, for other problems, in which $\nu \not\equiv 0$, the solution may not be separable and, if it is, the actual lateral eigenfunctions will differ from (21); consequently, we expect some errors in the method.

4.2 Angular spectrum approach

In Cartesian coordinates, the angular spectrum method and the Fourier-Galerkin approach are the same. However, in other coordinate systems, this may not be true. The angular spectrum method is then interpreted as an eigenfunction expansion method, with the eigenfunctions determined by the lateral Sturm-Liouville problem (20). The advantage of the angular spectrum method is that the lateral eigenfunctions are the exact solutions for the problem. The disadvantage of the method in transformed coordinates is that it is unlikely that there are fast algorithms (equivalent to the FFT) for obtaining eigenfunction expansions.

4.3 Chebyshev-tau approach

It is known that the Chebyshev polynomials, $T_n(\zeta)$, $n = 0, 1, 2, \ldots$, are a complete orthogonal basis over the range $-1 \leq \zeta \leq 1$. Their use requires a preliminary scaling of the problem,

$$\zeta = v/v_b,$$

so that the lateral boundaries are located at $\zeta = \pm 1$. The appropriate Chebyshev-transform pair is (cf. (12) and (13)):

$$c_n(u) = \mathcal{T}_C[\phi(u,v)] = \frac{\epsilon_n}{\pi} \int_{-1}^{1} \frac{\phi(u, v_b\zeta)\, T_n(\zeta)}{\sqrt{1-\zeta^2}}\, d\zeta, \quad n = 0, 1, 2, \ldots, \tag{37}$$

$$\phi(u,v) = \mathcal{T}_C^{-1}[c(u)] = \sum_{n=0}^{\infty} c_n(u)\, T_n(\zeta) \qquad \text{for } -1 < \zeta < 1. \tag{38}$$

As the Chebyshev polynomials do not satisfy the lateral boundary conditions, a straightforward Galerkin technique is precluded. The tau method forces the Chebyshev sum to satisfy these conditions, and will be discussed below.

Introducing $\overline{k^2 J}$ and ν, defined by (30) and (32), respectively, we find that the Chebyshev transform of (31) is

$$\frac{d^2 c_n(u)}{du^2} + \overline{k^2 J}\, c_n(u) + \frac{1}{v_b^2} c_n^{(2)} - \overline{k^2 J}\, \mathcal{T}_C[\nu\, \mathcal{T}_C^{-1}[c]] = 0.$$

The splitting in the transform domain follows as before:

$$\frac{dc_n^+}{du} = \left(\mathrm{i}\gamma_0 - \frac{1}{2\gamma_0}\frac{d\gamma_0}{du} \right) c_n^+(u) + \frac{\mathrm{i}}{2\gamma_0} \left(\frac{1}{v_b^2} c_n^{(2)} - \overline{k^2 J}\, \mathcal{T}_C[\nu\, \mathcal{T}_C^{-1}[c^+]] \right) = 0. \tag{39}$$

This equation is less accurate than that obtained from the Fourier-Galerkin splitting. Note that the first term on the right-hand side of (39) is proportional to γ_0 instead of γ_n, as the second derivative of T_n does not yield a term proportional to c_n directly as occurs with the trigonometric functions in the Fourier-Galerkin approach.

At $|\zeta| = 1$, $\partial\phi/\partial\zeta = 0$ so as to satisfy the no-flow channel boundary conditions. Since the Chebyshev polynomials do not satisfy these lateral boundary conditions individually (as the Fourier modes do), we use the Chebyshev-tau method to enforce them [5]. First, truncate the series in (38) to give

$$\phi(u,v) = \sum_{n=0}^{N} c_n(u)\, T_n(\zeta).$$

With this approximation, the no-flow conditions at $\zeta = \pm 1$ yield

$$\sum_{n=1}^{N} n^2 c_n(u) = 0 \qquad \text{and} \qquad \sum_{n=1}^{N} (-1)^n n^2 c_n(u) = 0.$$

These two equations are used to specify $c_{N-1}(u)$ and $c_N(u)$ in terms of the remaining coefficients, which are themselves determined by integrating (39) for $0 \leq n \leq N-2$; we used

a fourth-order Runge-Kutta scheme. The step size du depended on the number of modes computed, with a smaller step size required for a solution with more modes.

The Chebyshev transforms are carried out numerically using Gauss quadrature:

$$\int_{-1}^{1} \frac{g(\zeta)}{\sqrt{1-\zeta^2}} d\zeta \simeq \sum_{i=1}^{M} w_i \, g(\zeta_i)$$

The Gauss points ζ_i are the zeros of $T_M(\zeta)$, namely

$$\zeta_i = \cos\left(\frac{(2i-1)\pi}{2M}\right) \qquad i = 1, 2, \ldots, M$$

and $w_i = \pi/M$ for all i [1, Chap. 25]. For all calculations in this paper, $M = 41$, so that the quadrature error is negligible.

5 Diverging channel

For the case of the diverging channel, the angular spectrum, Fourier-Galerkin and Chebyshev-tau methods will be compared to the exact solution, which is given by (22) and (23).

5.1 Fourier-Galerkin and angular spectrum models

With the mapping that we have used, $w = \ln(z/r_0)$, the product $k^2 J$ is independent of v and so $\nu \equiv 0$; therefore, the last term in the equation for the Fourier modes (36) vanishes. The remaining terms (with the superscript + dropped for convenience) can be written as

$$\frac{df_n(u)}{du} = \left(\mathrm{i}\gamma_n - \frac{1}{2\gamma_n^2} k^2 r_0^2 \, \mathrm{e}^{2u}\right) f_n(u), \qquad n = 0, 1, 2, \ldots, \tag{40}$$

where

$$\gamma_n = \sqrt{k^2 r_0^2 \, \mathrm{e}^{2u} - \beta_n^2},$$

since $\lambda_n = \beta_n = \frac{1}{2} n\pi/\theta_\ell$.

For this case, modes not present in the initial conditions can not arise subsequently. Further, the Fourier cosine series in the lateral direction used in the Fourier transforms (33) and (34) are exact solutions of the associated Sturm-Liouville problem in the v-direction, guaranteeing convergence and also showing the equivalence of the Fourier-Galerkin and the angular spectrum (eigenfunction expansion) approaches for this case.

Equation (40) is a first-order equation for each of the Fourier modes. It can be solved analytically to give

$$f_n(u) = g_n \gamma_n^{-1/2} \exp\{\mathrm{i}(\gamma_n - \beta_n \tan^{-1}(\gamma_n/\beta_n))\}, \qquad n = 0, 1, 2, \ldots, \tag{41}$$

and then the potential is found from the inverse transform, (34). Note that, for large u and fixed n, we have $\gamma_n \sim k r_0 \mathrm{e}^u = kr$ and

$$f_n(u) \sim g_n (kr)^{-1/2} \exp\{\mathrm{i}(kr - \beta_n \pi/2)\},$$

which is the far-field approximation to $H^{(1)}_{\beta_n}(kr)$, apart from a constant factor. Therefore, we expect an exact correspondence among the angular spectrum method, the Fourier-Galerkin method, and the exact linear solution for this example.

5.2 Chebyshev-tau method

From (39), the governing equation for each of the Chebyshev modes is

$$\frac{dc_n(u)}{du} = \left(\mathrm{i}\gamma_0 - \frac{1}{2}\right) c_n(u) + \frac{\mathrm{i}}{2v_b^2\gamma_0} c_n^{(2)} = 0, \qquad n = 0, 1, 2, \ldots. \tag{42}$$

For the case of normal wave incidence, the solution is symmetric about $\zeta = 0$, and so the coefficients of all the odd Chebyshev polynomials are zero.

5.3 Results

One possible wave motion in the diverging channel is the axisymmetric case of circular waves emanating from $r = 0$, with constant amplitude and phase along any circular arc. The initial condition is taken as $G(\theta) = 1$. The linear wave motion is given analytically in (22) and most conveniently by the leading term, the Hankel function, $H_0^{(1)}(kr)$, where $r = \sqrt{x^2 + y^2}$. All of the numerical methods model this solution correctly in the far field, giving

$$\phi(u, v) = \exp\left(\mathrm{i}k\mathrm{e}^u - \tfrac{1}{2}u\right),$$

which is the far-field expansion of the Hankel function. In the mapped domain, the wave form is constant along lines of constant u, and no diffraction occurs.

On the other hand, if a plane wave enters the diverging channel, then diffraction occurs as the physical domain becomes wider in the propagation direction. This situation was modelled by Kaku and Kirby [13] in a wave tank (see also the description in [19]). In a water depth of 0.15 m, vertical plywood breakwaters enclosed a 90° sector, with a mouth of width 1.74 m. A planar wave generator sent waves directly down the centerline. Measurements were made using wavegages at fixed r locations for several wave cases. Here, we use the most linear set of tests for which the wave period was 0.49 s, and the initial wave amplitude was 0.0085 m. The measurement stations correspond to $r/r_0 = (1.38, 1.87, 2.2)$, where $r_0 = 1.23$ m, taken as the distance from the origin of the polar coordinate system to the breakwaters, and at 10° increments from the centerline.

For the models, the plane wave initial condition of $\phi = \exp(\mathrm{i}kr_0\cos\theta)$ was used. In figure 2, the exact water surface elevation is shown for the data of Kaku and Kirby [13] in the transformed domain, where there is apparent focussing of the wave form down the centerline, which is due to the widening of the channel with r in the physical domain. In figure 3, the angular spectrum (Fourier-Galerkin) model predictions for water surface elevations are compared to the exact theory and the data from [13]. The Fourier-Galerkin model gives, as expected, the same result as the exact solution. In comparing to the parabolic models of [19], the Fourier-Galerkin model is better, as the parabolic models do not replicate the exact theory.

The Fourier-Galerkin model was run with a step size corresponding to $k\,dr = 0.2136$, where, for this water depth and wave period, the dispersion relationship (2) gives $k = 16.94\ \mathrm{m}^{-1}$. Only the seven progressive modes were used.

For the Cheybshev-tau model, 15 even modes were used ($N = 28$). For this high number of modes, a very small step size in u was necessary, $du = 0.001787$; this required about

500 steps to span the measurement locations – more than required by the Fourier-Galerkin method by almost a factor of three. In figure 4, the Chebyshev solution is compared to the data from [13] and to the exact solution. Clearly, there is a discrepancy between the Chebyshev solution and the exact solution, due to the presence of a lateral oscillation in the solution.

6 Circular channel

The exact linear solution for this case is given by (28), with (27) and (29). Again, the Fourier-Galerkin and the Chebyshev-tau methods will be compared against this exact solution. In the following examples, the initial condition is a wave train with constant amplitude across the channel, or $G = 1$ in (29).

6.1 Fourier-Galerkin model

As J is not a function of u for this case, the governing equation (36) reduces to

$$\frac{df_n(u)}{du} = \mathrm{i}\gamma_n f_n - \frac{\mathrm{i}\,\overline{k^2 J}}{2\gamma_n}\mathcal{T}_F[\nu\,\mathcal{T}_F^{-1}[f]], \qquad n = 0, 1, 2, \ldots \tag{43}$$

where

$$\overline{k^2 J} = \frac{k^2\,(r_2^2 - r_1^2)}{2\ln(r_2/r_1)} \qquad \text{and} \qquad \nu(v) = 1 - \frac{2\ln(r_2/r_1)\,r_1 r_2 \mathrm{e}^{-2v}}{r_2^2 - r_1^2},$$

since $v_b = \frac{1}{2}\ln(r_2/r_1)$. Now, the Fourier modes, $\{\cos[\lambda_n(v + v_b)]\}$, $n = 0, 1, 2, \ldots$, no longer satisfy the exact Sturm-Liouville problem in the lateral direction, which is (25) together with $V'(\pm v_b) = 0$; the Fourier-Galerkin method no longer is the same as the angular spectrum method and the method will have problems with convergence, depending on the size of ν; we have

$$1 - \frac{2r_2^2 \ln(r_2/r_1)}{r_2^2 - r_1^2} \le \nu(v) \le 1 - \frac{2r_1^2 \ln(r_2/r_1)}{r_2^2 - r_1^2} \qquad \text{for } r_1 \le r \le r_2.$$

6.2 Angular spectrum model

The actual lateral eigenfunctions for this problem are given by (27). The propagating modes are given by (24). For the present case of a constant depth channel, the angular spectrum and the exact solution are identical.

6.3 Chebyshev model

The governing equation is obtained from (39):

$$\frac{dc_n(u)}{du} = \mathrm{i}\gamma_0 c_n(u) + \frac{\mathrm{i}}{2\gamma_0}\left(\frac{1}{v_b^2}c_n^{(2)} - \overline{k^2 J}\,\mathcal{T}_C[\nu\,\mathcal{T}_C^{-1}[c]]\right) = 0 \tag{44}$$

with

$$\overline{k^2 J} = \frac{k^2 r_1 r_2}{2v_b}\sinh(2v_b).$$

6.4 Results

6.4.1 Narrow channel

A narrow channel is defined as a channel with a width smaller than the wavelength of the incident wave, or $k(r_2 - r_1) < 2\pi$, where the left-hand side is 2π times the number of wavelengths that can fit across the channel. This can be rewritten as $kr_1\delta < 2\pi$, where δ is the dimensionless channel width: $\delta = (r_2 - r_1)/r_1$. In a narrow channel, the waves propagate around the channel with very little change in wave form. For example, given $r_1 = 75$ m, $r_2 = 80$ m, a water depth of 4 m and a wave period of 4 seconds, $kr_1\delta = 1.5$ and the wave propagates within the channel with little change in form (the wave amplitude along the outside wall is only 3% greater than elsewhere). The numerical models and the analytic (exact) model (with only one progressive mode) are indistinguishable for this case.

6.4.2 Wider channel

For a wider channel, obtained by increasing r_2 to 100 m, $kr_1\delta = 7.53$, which corresponds to a channel wider than a wavelength. For this case, the wave field is significantly different, largely due to the much greater distance encompassed by the outer radius than the inner. The ratio of the distances (circumferences) is $r_2/r_1 = \delta + 1$, which is 1.33 in this case; therefore, δ measures the percentage increase in length of the outer circumference over the inner one, or it is a measure of the longer path followed by waves on the outer side of the channel than the inside. Figure 5 shows an instantaneous snapshot in the conformal domain of the free surface (analytical model), which is comprised of the three progressive modes. Of particular note is the so-called amphidromic point in the wave phase that occurs where the 'extra' wave appears along the outer radius (to the right on the figure); for a discussion of these special points, see [22].

Figure 6 shows the water surface elevation along the outer circumference as predicted by the Fourier-Galerkin model and the analytical model for $0° \leq \theta \leq 90°$. The agreement is quite good, with the Fourier-Galerkin model slightly underpredicting the maxima and propagating slightly faster than the exact solution. For this case, $\overline{k^2 J} = 689.8$.

In Figure 7, the three lateral eigenfunctions comprising the analytical solution (28) are shown. In comparison, the Fourier cosines for the Fourier-Galerkin model are shown in Figure 8. The difference between the general shapes of the eigenfunctions is not large; however, the behavior of the coefficients multiplying these eigenfunctions is very different. For the analytical model, the a_n values are constant, and the variation of the wave form with θ is due to the superposition of the different modes comprising the solution. For the Fourier-Galerkin model, with its imperfect Fourier series, the Fourier coefficients exchange energy along the channel according to (43).

The Chebyshev-tau comparison for the water surface elevation along the outer wall is shown in Figure 10. Ten Chebyshev polynomials were used for this solution; the use of only eight polynomials gives the same solution.

6.4.3 Wide channel

Waves in a very wide channel begin to experience diffraction and strong reflection. For this example, $r_2 = 200$ m, so $kr_1\delta = 37.6$, and $\delta = 1.67$. The analytic solution has 12 progressive modes for this case. The waves in the wide (six wave lengths) circular channel initially propagate in a straight line, but as the channel bends, the waves start to diffract around the bend and simultaneously run into the curving channel sidewall to reflect around the bend. Different parts of the wave crest reflect at different times, leading to a complicated sea-state far along the channel. The instantaneous water surface from the exact solution in the physical domain is shown in Figure 11. The water surface is shown in the conformal domain in Figure 12.

The Fourier-Galerkin model does not yield a very good solution for this case, due to the large variation in k^2J over the channel width. The Fourier-Galerkin method assumes that the lateral variation of the solution is expressible in terms of the Fourier series in the v coordinate (which look similar to those in Figure 8). The actual shapes of the eigenfunctions (obtained from the exact solution) are shown in Figure 13 and are those used in the angular spectrum model. The very different nature of these eigenfunction imply that trigonometric bases is not efficient for this case.

The water surface elevations along the outer wall computed by the Fourier-Galerkin model are compared to the exact solution in Figure 14. Clearly, there is a discrepancy, with the Fourier-Galerkin waves having a faster phase variation than the exact solution. The largest discrepancy occurs at about 38° . (The numerical model was run with grid sizes: du=0.452° , dv=0.0377°).

Figure 15 shows the water surface elevations on the outer wall as predicted by the Chebyshev-tau model for the wide channel. Here, $N = 20$, $M = 41$ and $du = d\theta = .00394$ radians. Clearly, the model has a phase error, which leads to wide discrepancies at 45° . It is likely that this error is largely due to the errors developed in the splitting process and the correspondence to the small-angle parabolic model, which is exacerbated in this case due to the variable nature of k^2J. Kirby *et al.* [19] show that a small-angle parabolic model actually does better than shown here for the Chebyshev-tau model, and that the large angle parabolic model does better than all of these forward-propagating spectral solutions.

7 Discussion

In Cartesian coordinates, the angular spectrum model, the eigenfunction expansion method (separation of variables), and the Fourier-Galerkin model are identical. In conformal domains, this is not necessarily true. The angular spectrum model is interpreted as an expansion of the velocity potential in terms of the eigenfunctions in the lateral (v) direction. These eigenfunctions are found by separation of variables, (20). For the Fourier-Galerkin method, the lateral eigenfunctions for a channel are a Fourier cosine series, while for the Chebyshev-tau method, the lateral functions are Chebyshev polynomials.

For the case of the diverging channel, the lateral eigenfunctions turn out to be cosines; therefore, for this case also, the Fourier-Galerkin method and the angular spectrum method are the same. The Chebyshev-tau method, however, does not approach the exact solution

analytically and, numerically, it is not as accurate as the Fourier-Galerkin method.

For the case of an annular channel, the angular spectrum model (using the eigenfunctions given by (27)), coincides with the exact solution, while the Fourier-Galerkin method is shown to become more inaccurate as the channel width increases. The Fourier cosine series differs drastically from the actual lateral eigenfunctions for the wide channel case. This is also true for the Chebyshev-tau forward-propagation model. The source of the errors is the increasing size of ν, which causes the last term in (43) and in (44) to become large. Clearly, the use of the mean value of $k^2 J$ does not properly model the behavior of the waves for these large ν cases.

Extension of these models to variable depths is relatively simple, as the variable depth case is treated by a variable coefficient Helmholtz equation, as discussed in [19].

Acknowledgments

R.A.D. and J.T.K. were supported, in part, by NOAA Office of Sea Grant, Department of Commerce, under Grant No. NA/16RG0162-03 (Project No. R/OE-12 (RAD) and R/OE-13 (JTK)). The U.S. Government is authorized to produce and distribute reprints for governmental purposes, notwithstanding any copyright notation that may appear hereon.

We would like to thank John P. Boyd for helpful comments on the implementation of the Chebyshev approach.

Appendix. Conformal transformation

To determine the governing equation in the transformed domain, the chain rule operators

$$\frac{\partial}{\partial x} = \frac{\partial u}{\partial x}\frac{\partial}{\partial u} + \frac{\partial v}{\partial x}\frac{\partial}{\partial v}, \qquad \frac{\partial}{\partial y} = \frac{\partial u}{\partial y}\frac{\partial}{\partial u} + \frac{\partial v}{\partial y}\frac{\partial}{\partial v} \tag{A.1}$$

are used. Applying these to ϕ for first derivatives, applying them again to obtain the second derivatives, and, finally, substituting into the governing equation (1) yields

$$(\nabla u)^2 \frac{\partial^2 \phi}{\partial u^2} + 2\nabla u \cdot \nabla v \frac{\partial \phi}{\partial uv} + (\nabla v)^2 \frac{\partial^2 \phi}{\partial v^2} + \nabla^2 u \frac{\partial \phi}{\partial u} + \nabla^2 v \frac{\partial \phi}{\partial v} + k^2 \phi = 0. \tag{A.2}$$

While the derivatives of ϕ in this equation are taken with respect to the mapped coordinates, the coefficients still involve derivatives of u and v with respect to x and y. Applying both operators (A.1) to dx, we obtain

$$1 = \frac{\partial u}{\partial x}\frac{\partial x}{\partial u} + \frac{\partial v}{\partial x}\frac{\partial x}{\partial v} \qquad \text{and} \qquad 0 = \frac{\partial u}{\partial x}\frac{\partial y}{\partial u} + \frac{\partial v}{\partial x}\frac{\partial y}{\partial v}.$$

This pair of equations can be easily solved to give

$$\frac{\partial u}{\partial x} = \frac{1}{J}\frac{\partial y}{\partial v} \tag{A.3}$$

$$\frac{\partial v}{\partial x} = \frac{1}{J}\frac{\partial y}{\partial u} \tag{A.4}$$

where J is the Jacobian, defined by (18). The same procedure is repeated for dy, resulting in

$$\frac{\partial u}{\partial y} = -\frac{1}{J}\frac{\partial x}{\partial v} \tag{A.5}$$

$$\frac{\partial v}{\partial y} = \frac{1}{J}\frac{\partial x}{\partial u} \tag{A.6}$$

For a conformal mapping, the Cauchy-Riemann conditions are required to ensure that the transformation is holomorphic (that is, derivatives exist everywhere). These are

$$\frac{\partial u}{\partial x} = \frac{\partial v}{\partial y} \quad \text{and} \quad \frac{\partial u}{\partial y} = -\frac{\partial v}{\partial x}.$$

By taking derivatives of these expressions, it is straightforward to show that $\nabla^2 u = 0$ and $\nabla^2 v = 0$. Furthermore, by substituting from (A.4) and (A.6), the Cauchy-Riemann conditions show that

$$\frac{\partial x}{\partial u} = \frac{\partial y}{\partial v} \quad \text{and} \quad \frac{\partial x}{\partial v} = -\frac{\partial y}{\partial u}.$$

Utilizing the last two sets of conditions, the general curvilinear coordinate system governing equation (A.2) is greatly simplified to one valid for conformal coordinate systems: the result is (17).

References

[1] M Abramowitz and I. A. Stegun, *Handbook of Mathematical Functions*, Dover, New York, 1965.

[2] H. G. Booker and P. C. Clemmow, *The concept of an angular spectrum of plane waves, and its relation to that of polar diagram and aperture distribution*, Proc. Inst. Elect. Engrs., 97 (1950), pp. 11–17.

[3] J. P. Boyd, *Chebyshev and Fourier Spectral Methods*, Springer, Berlin, 1989.

[4] H. Buchholz, *Der Einfluss der Krümmung von rechteckigen Hohlleitern auf das Phasenmass ultrakurzer Wellen*, Electrische Nachrichtentechnik, 16 (1939), pp. 73–85.

[5] C. Canuto, M. Y. Hussaini, A. Quarteroni and T. A. Zang, *Spectral Methods in Fluid Dynamics*, Springer, Berlin, 1988.

[6] R. A. Dalrymple, *Water waves past abrupt channel transitions*, Applied Ocean Research, 11 (1989), pp. 170–175.

[7] R. A. Dalrymple and M. D. Greenberg, *Directional wavemakers*, in Physical Modelling in Coastal Engineering, R. A. Dalrymple, ed., Balkema, Rotterdam, 1984, pp. 67–79.

[8] R. A. Dalrymple and J. T. Kirby, *Models for very wide angle water waves and wave diffraction*, J. Fluid Mech., 192 (1988), pp. 33–50.

[9] R. A. Dalrymple and J. T. Kirby, *Angular spectrum modelling of water waves*, Reviews in Aquatic Sciences, 6 (1992), pp. 383–404.

[10] R. A. Dalrymple and P. A. Martin, *Wave diffraction through offshore breakwaters*, J. Waterway, Port, Coastal & Ocean Engrg., 116 (1990), pp. 727–741.

[11] R. A. Dalrymple, K. D. Suh, J. T. Kirby and J. W. Chae, *Models for very wide angle water waves and wave diffraction, Part 2. Irregular bathymetry*, J. Fluid Mech., 201 (1989), pp. 299–322.

[12] J. D. Hoffman, *Numerical Methods for Engineers and Scientists*, McGraw-Hill, New York, 1992.

[13] H. Kaku and J. T. Kirby, *A parabolic equation method in polar coordinates for waves in harbors*, Tech. Rept. UFL/COEL-TR/075, Coastal and Ocean Engrg. Dept., Univ. Florida, Gainesville, 1988.

[14] J. M. Kaihatu and J. T. Kirby, *Spectral evolution of directional finite amplitude dispersive waves in shallow water*, Proc. 23rd Int. Coastal Engrg. Conf., ASCE, Venice, 1992, pp. 364–377.

[15] J. T. Kirby, *Parabolic wave computations in non-orthogonal coordinate systems*, J. Waterway, Port, Coastal and Ocean Engrg., 114 (1988), pp. 673–685.

[16] J. T. Kirby, *Modelling shoaling directional wave spectra in shallow water*, Proc. 22nd Int. Coastal Engrg. Conf., ASCE, Delft, 1990, pp. 109–122.

[17] J. T. Kirby and R. A. Dalrymple, *A parabolic equation for the combined refraction-diffraction of Stokes waves by mildly varying topography*, J. Fluid Mech., 136 (1983), pp. 453–466.

[18] J. T. Kirby and R. A. Dalrymple, *Documentation Manual, Combined Refraction/Diffraction Model, REF/DIF 1*, Version 2.4, Center for Applied Coastal Research, Res. Rpt. CACR-92-04, 1992.

[19] J. T. Kirby, R. A. Dalrymple and H. Kaku, *Parabolic approximations for water waves in conformal coordinate systems*, Coastal Engineering, in press, 1994.

[20] C. Lanczos, *Applied Analysis*, Prentice-Hall, Englewood Cliffs, 1956.

[21] P. L. -F Liu and P. L. Boissevain, *Wave propagation between two breakwaters*, J. Waterway, Port, Coastal and Ocean Engrg., 114 (1988), pp. 237–247.

[22] P. A. Martin and R. A. Dalrymple, *On amphidromic points*, Proc. Roy. Soc. London Ser. A, in press, 1994.

[23] V. G. PANCHANG AND D. A. KOPRIVA, *Solution of two-dimensional water-wave propagation problems by Chebyshev collocation*, Mathl. Comput. Modelling, 12 (1989), pp. 625–640.

[24] A. C. RADDER, *On the parabolic equation method for water-wave propagation*, J. Fluid Mech., 95 (1979), 159–176.

[25] W. ROSTAFINSKI, *Acoustic systems containing curved duct sections*, J. Acoust. Soc. Amer., 60 (1976), pp. 23–28.

[26] J. J. STAMNES, O. LØVHAUGEN, B. SPJELKAVIK, C. C. MEI, E. LO AND D. K. P. YUE, *Nonlinear focusing of surface waves by a lens – theory and experiment*, J. Fluid Mech., 135 (1983), pp. 71–94.

[27] K. D. SUH AND R. A. DALRYMPLE, *Application of the angular spectrum model to simulation of irregular wave propagation*, J. Waterway, Port, Coastal and Ocean Engineering, 119 (1993), pp. 505–519.

[28] K. D. SUH, R. A. DALRYMPLE AND J. T. KIRBY, *An angular spectrum model for propagation of Stokes waves*, J. Fluid Mech., 221 (1990), pp. 205–232.

[29] J. F. THOMPSON, *Numerical Grid Generation*, North-Holland, Amsterdam, 1982.

[30] L. N. TREFETHEN, ed., *Numerical Conformal Mapping*, North-Holland, Amsterdam, 1986.

[31] T. -K. TSAY, B. A. EBERSOLE AND P. L. -F. LIU, *Numerical modelling of wave propagation using parabolic approximation with a boundary-fitted co-ordinate system*, Internat. J. Numer. Methods Engrg., 27 (1989), pp. 37–55.

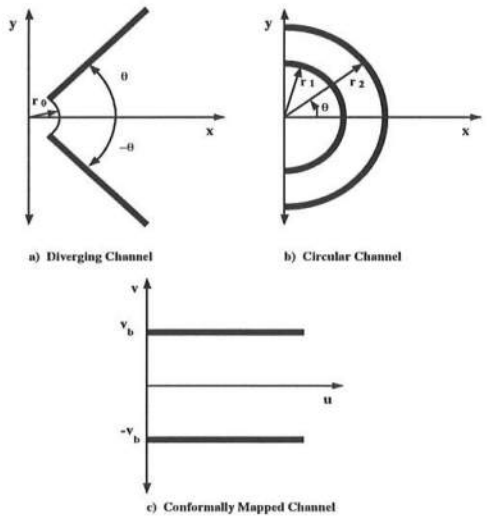

Figure 1: Schematic Diagram of the Two Examples (top row, a,b) and the Conformed Channel (c).

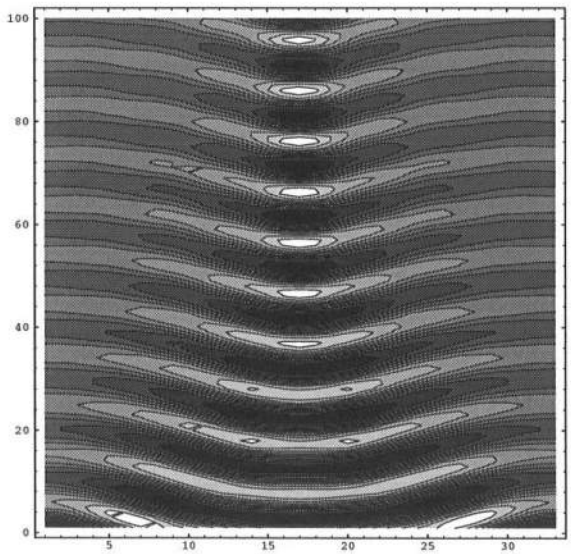

Figure 2: Instantaneous Water Surface of Diverging Channel in Mapped Domain

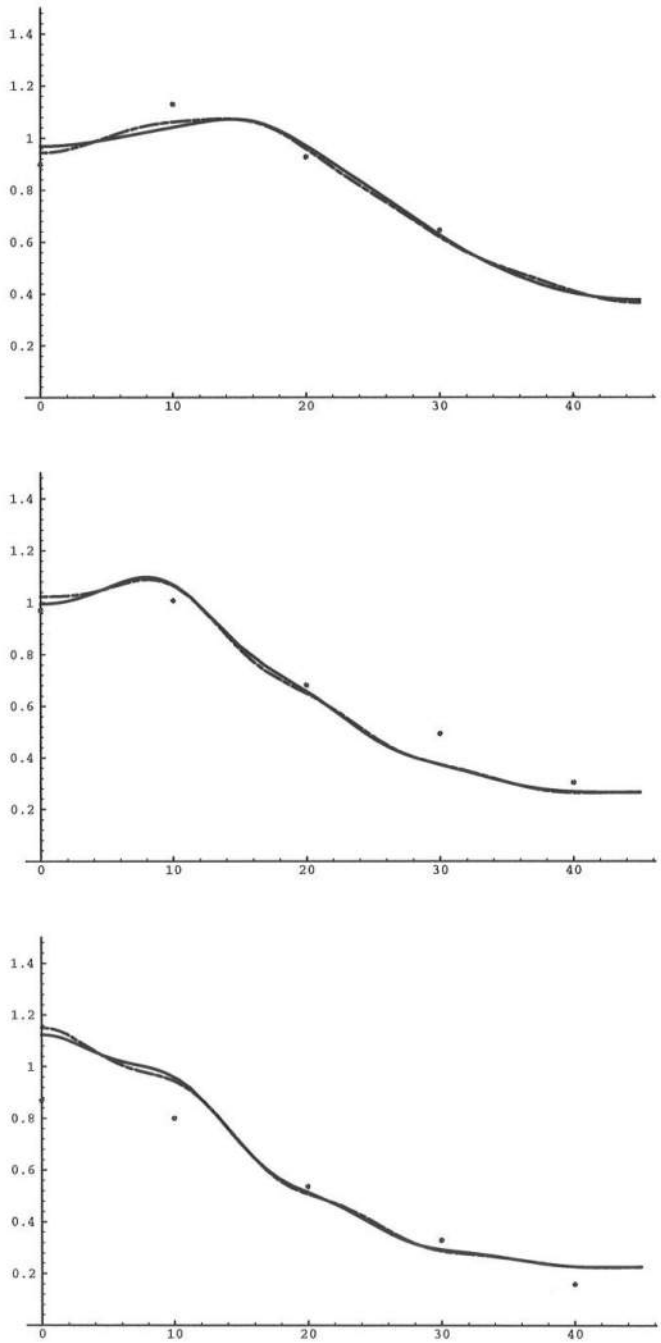

Figure 3: Comparisons of the Angular Spectrum Model (dashed line), the Exact Solution (solid line) and the Data of Kaku and Kirby (1988) at r=1.38, 1.87, 2.2m from top figure to bottom.

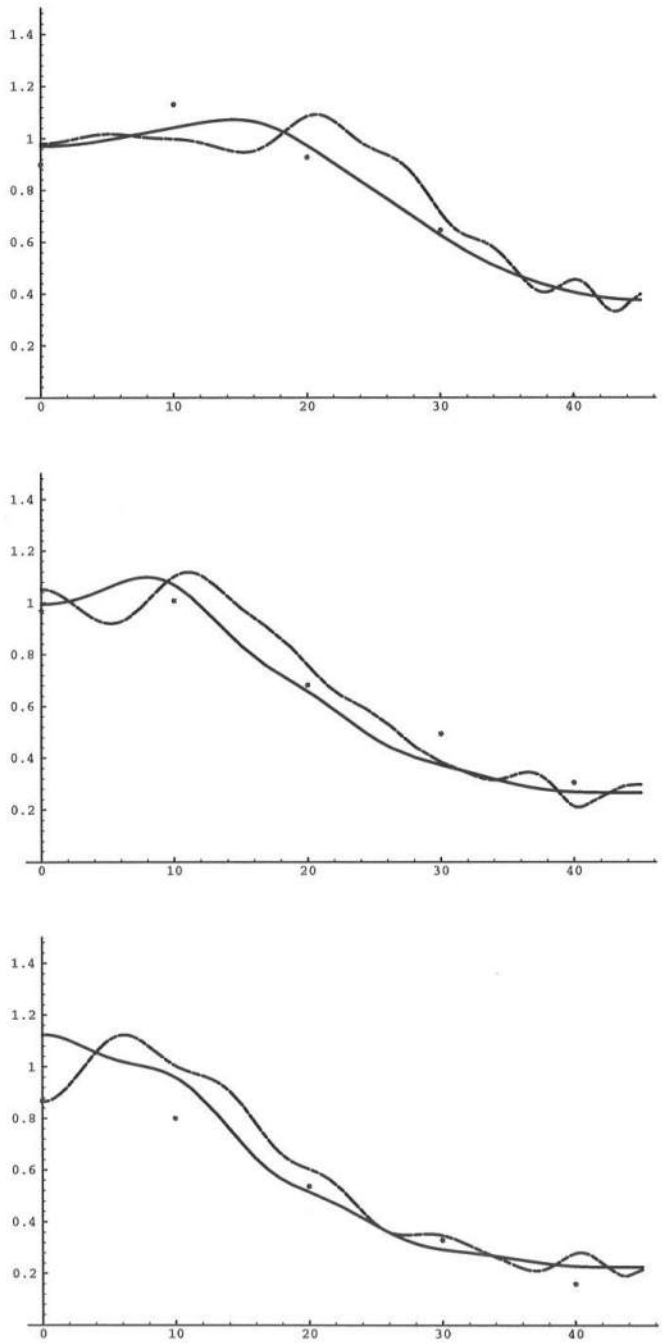

Figure 4: Comparisons of the Chebyshev Model (dashed line), the Exact Solution (solid line) and the Data of Kaku and Kirby (1988) at r=1.38, 1.87, 2.2m from top figure to bottom.

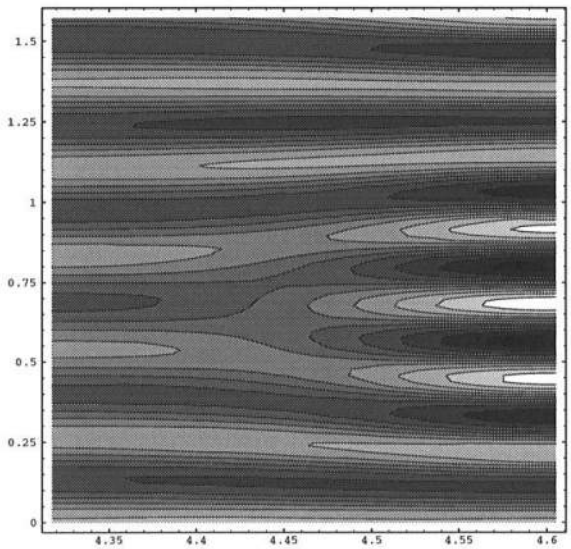

Figure 5: Exact Solution in (u, v) Plane for Waves in a Wider Circular Channel

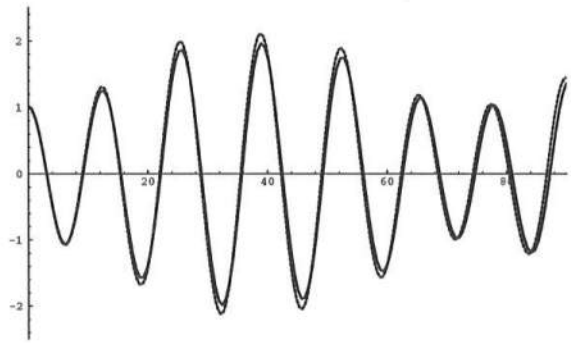

Figure 6: Comparison of Water Surface Elevation along Outer Wall Between the Exact Solution and the Fourier–Galerkin Model (dashed line) for Wider Channel

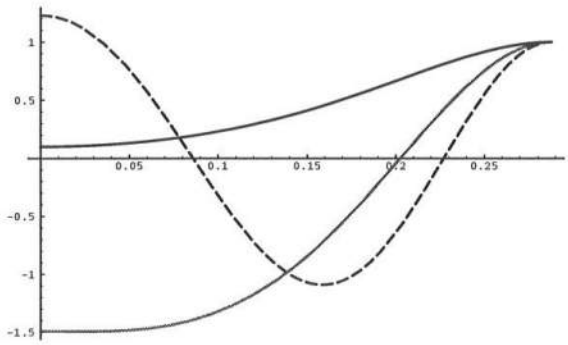

Figure 7: Three Analytical Eigenfunctions for the Wider Channel

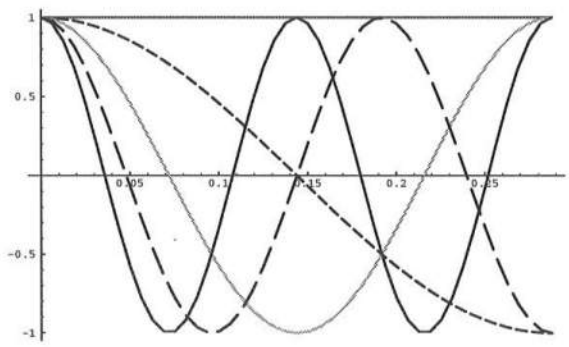

Figure 8: Eigenfunctions for Waves in a Wider Circular Channel in Angular Spectrum Model

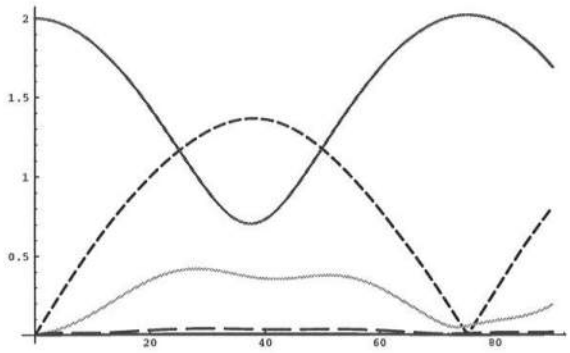

Figure 9: Variation of the First Five Fourier Modes in the Wider Channel as a Function of Angle

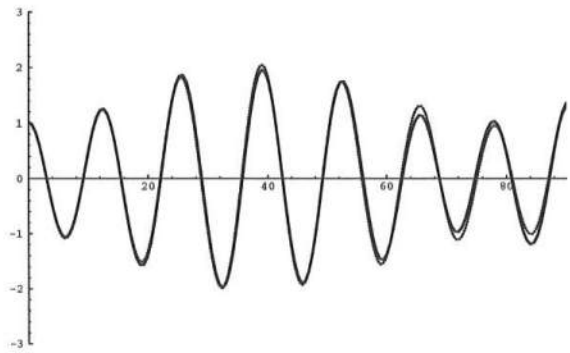

Figure 10: Comparison of Water Surface Elevation along Outer Wall Between the Exact Solution and the Chebyshev–tau Model (dashed line) for Wider Channel

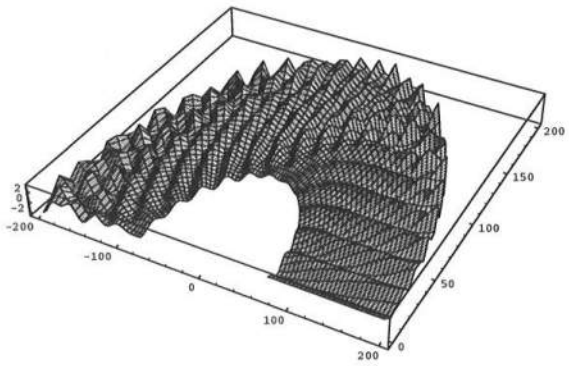

Figure 11: Exact Solution for Waves in a Wide Circular Channel

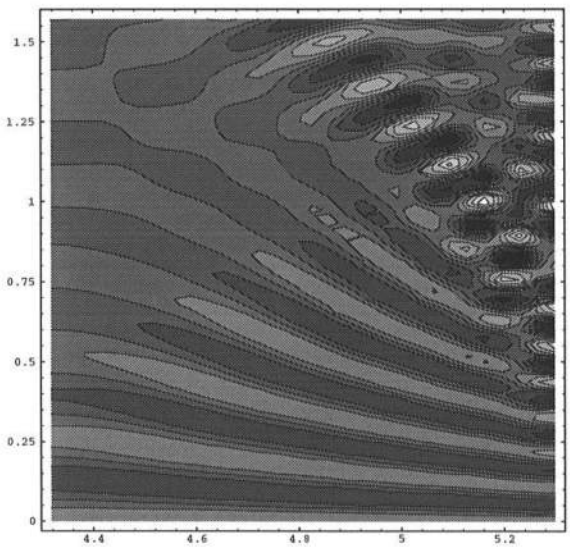

Figure 12: Exact Solution for Waves in a Wide Circular Channel in the Transform Domain

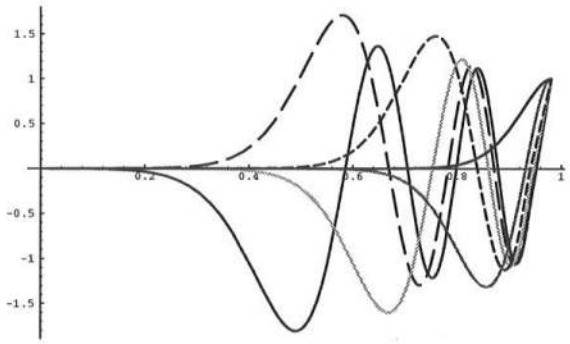

Figure 13: Analytic Eigenfunctions for Waves in a Wide Circular Channel

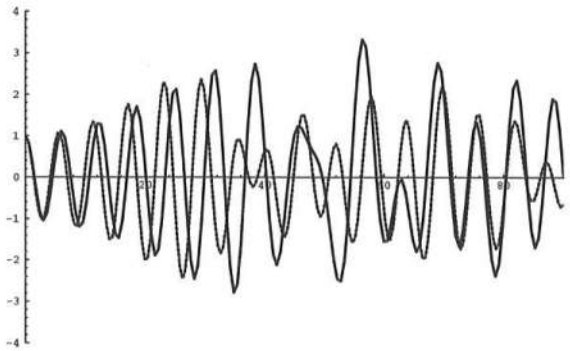

Figure 14: Comparison of the Water Surface Variation Along Outer Wall Between the Exact Solution (solid line) and the Fourier-Galerkin Model (dashed line)

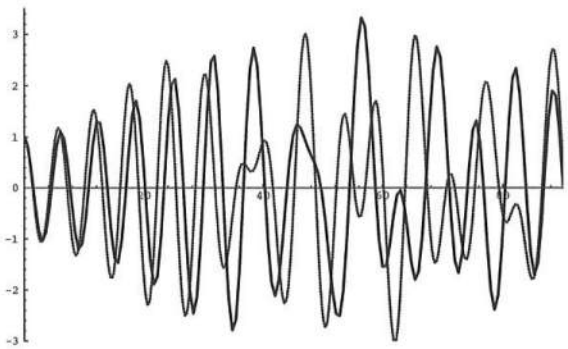

Figure 15: Comparison of the Water Surface Variation Along Outer Wall Between the Exact Solution (solid line) and the Chebyshev-tau Model (dashed line)